Received: 23 April 2021 | Revised: 1 October 2021 | Accepted: 11 November 2021

DOI: 10.1002/we.2697

RESEARCH ARTICLE

WILEY

The significance of bypass transition on the annual energy production of an offshore wind turbine

Aidan Duffy | Grant Ingram | Simon Hogg

Department of Engineering, Durham University, Durham, UK

Correspondence
Aidan Duffy, Department of Engineering, Durham University, Durham DH1 3LE, UK.
Email: aidan.j.duffy@durham.ac.uk

Funding information
EPSRC Prosperity Partnership: A New Partnership in Offshore Wind

Abstract

Awareness of leading-edge erosion (LEE) on wind turbine blades, and the impacts it can have on annual energy production (AEP) have increased significantly over recent years. This is especially important in offshore environments, where a combination of more extreme weather and higher tip speeds result in higher rates of erosion. In this paper the impact of LEE on AEP has been quantified and the derived method validated. The DTU 10-MW reference wind turbine (RWT) is used to demonstrate the method. An equivalent sand grain roughness approach in computational fluid dynamics (CFD) is used to simulate clean and roughened aerofoil performance. These CFD results are applied to a blade element momentum (BEM) model of the turbine to generate clean and eroded power curves. Finally, a wind distribution from Anholt offshore wind farm is used to estimate the AEP for the clean and eroded cases. An AEP loss of 0.7% was computed for the specific case considered in this study. This result is benchmarked against those from previously published studies. Most research into LEE has thus far focussed on either estimating the impacts on AEP or mitigating against them, with less emphasis on understanding the physical aerodynamic changes that result in reduced energy output. In this paper, the significance of bypass transition on the AEP loss caused by roughness, specifically as it relates to the operational angles of attack of the blade, is examined and found to impact turbine efficiency in this case for over 56% of the total operating time.

KEYWORDS
annual energy production, bypass transition, leading edge erosion

1 | INTRODUCTION

It is now recognised that the offshore wind sector has a major role to play in decarbonising electricity generation, particularly in countries with relatively shallow coastal waters such as the UK. The rapid growth in wind turbine size over the last decade has placed offshore wind amongst the most economically viable sources of renewable power generation. The levelised cost of energy (LCoE) for offshore wind has decreased by over 50% between 2016 and 2019 for fixed foundation turbines, with projections of a further 40% reduction by 2030.[1] The continued decreases in LCoE will come from a number of sources, including technological advancements which will lead to increased power density (power output per unit rotor area) of wind turbines. Improving the understanding of blade erosion processes and their effect on turbine performance has a role to play in this respect. One of the significant benefits of offshore wind turbines compared to onshore, lies in the ability to use larger blade diameters

to achieve a higher power density, with higher permissible tip speeds due to fewer restrictions on noise emissions.[2] However, this has the undesirable effect of increasing the kinetic energy at which particulate matter, such as rain droplets, impinge on the blade surfaces, resulting in enhanced rates of blade erosion compared to an onshore environment.[3] The understanding of erosion development is consistent across literature. It begins with small pits, where material is chipped away by repetitive impacts. Over time, these coalesce into larger and deeper gouges, before exposing the laminate. At this point, water ingress between the laminate layers begins, which eventually causes delamination.[4] However, while the process is well understood, categorisation is not consistent. For example, both Sareen et al.[4] and Gaudern[5] describe the erosion process as consisting of five stages, but define them using different parameters. This can lead to difficulties in comparing studies.

Increased leading edge (LE) erosion results in decreased aerodynamic efficiency of turbines, leading to a reduction in turbine power output, and in turn, the annual energy production (AEP). Several previously published studies have assessed this by running various types of aerofoil data through a BEM model. Sareen et al.[4] considered a range of roughness levels provided by 3 M, which were applied along the whole blade length, on the first 1%–3% of the chord length of an unspecified 2.5-MW turbine. No attempt was included in this study to consider the spanwise variations in erosion damage observed on operational turbines towards the blade tips, caused by the higher relative blade velocities in this region. Their predicted AEP losses due to erosion effects ranged from 4% to 24%. Veraart[6] employed statistical analysis techniques on rain erosion test samples to develop erosion distributions, encompassing depth, chord and span variations. Three aerofoil sections, roughened over the first 4% of their chord to simulate different levels of erosion, were applied to the outer 15% of the blade span. This study also used a 2.5-MW turbine, the details of which were not disclosed. The predicted AEP losses were in the range of 0.5%–1.8% and varied with mean wind speed, with a higher mean wind speed relating to a lower AEP loss. Eisenberg et al.[7] used an analytical approach to develop an erosion damage model. This was then applied using the erosion damage levels suggested by Sareen et al.[4] Their prediction of AEP loss, based on applying erosion damage to the outer 10% of a blade, was 1.7%. However, it is not clear whether the erosion damage was applied only in the LE region, or over the entire blade chord in this study. Schramm et al[8] also used the work of Sareen et al. to develop eroded LE sections for use in CFD analyses. Erosion was simulated on the outer 29.3% of the blades on the NREL 5-MW reference turbine. The results showed AEP losses of 7%–8%. However, the BEM model used in the study did not account for pitch control of the turbine blades. This caused much greater differences between clean and eroded power curves in the higher wind velocity region, compared to pitch-controlled units which maintain rated power at the higher wind speeds by altering blade pitch angle to reduce torque. This essentially removes any effects of erosion in this part of a turbine's power curve. A series of experiments assessing different roughness heights were undertaken by Langel et al.,[9] with roughness applied to the first 5% of the chord length, although seemingly not accounting for spanwise variations. The NREL 5-MW reference turbine was also used in the study. The predicted AEP losses were between 1.7% and 4.5%. Similar to Veraart, the results showed a dependency on mean wind speed. Han et al.[10] used the same turbine and analysed eroded configurations using CFD. Erosion damage was applied to the outer 29.3% of blades. By assessing a range of roughness heights and chordwise coverages, losses were predicted to lie between 2% and 3.7%. Bak et al.[11] used bumps or grooved sections at the LE of an aerofoil to simulate erosion in a CFD study. Erosion was simulated over a range of depths, and chordwise and spanwise penetrations, on a model of the Vestas V52 wind turbine. The predicted AEP loss was in the range of 0.5%–3%, depending upon the wind distribution used in the simulations and the erosion coverage applied to the blades. Chord and span penetration, along with erosion depth and roughness height were considered by Papi et al.[12] A series of probability density functions were developed from data on erosion parameters reported in literature, to establish a range of aerofoil sections with different levels of simulated erosion damage. The DTU 10-MW reference wind turbine (RWT) was used in the study. The mean AEP loss reported was 0.87%.

The presence of LE erosion on wind turbine blades can trigger bypass transition which can have a significant impact on AEP. Bypass transition occurs in the presence of roughness, or erosion, and causes the transition from laminar to turbulent flow to occur earlier than for natural transition mechanisms.[13] In a review of boundary layer transition by Tani,[14] the occurrence of a critical Reynolds number for bypass transition was identified. This was found to be dependent on angle of attack and roughness height. Ehrmann et al.[15] observed this experimentally by testing a range of roughness configurations. The results showed that bypass transition is also dependent on the coverage area and density of roughness, a factor which had been hypothesised previously by Morkovin.[16] Bypass transition is also an issue in other stages of a turbine's life, as shown by Major et al.[17] when using LE protection tapes. In assessing the aerodynamic impact of the step at the tape-aerofoil boundary it was shown that this acts much in the same way as roughness in initiating early transition, but that by tapering the end of the tape onto the aerofoil the bypass effect can be largely eliminated.

The results from the various studies described above show a variation in the predicted impact of blade erosion damage on wind turbine AEP, from 0.5% to 24%. This highlights the importance of accurately modelling erosion levels, that is, depth, roughness height, erosion density and the area of the blade surfaces affected by erosion damage, when calculating AEP loss. The work described in this paper was carried out in collaboration with Ørsted and Siemens Gamesa Renewable Energy (SGRE). Access to data and service experience from the two companies built up over several years on current generation offshore wind turbines has been used to inform the severity and extent of the blade erosion damage simulated in this study.

The key feature of this study is using realistic and representative inputs for AEP analyses in order to provide more accurate predictions for site specific cases of LE erosion. The research objectives are (i) validating a 2D CFD approach for predicting aerodynamic losses in the presence of distributed roughness; (ii) predicting the AEP loss from a case with established erosion; (iii) assessing the role that bypass

transition plays in decreasing aerodynamic efficiency; and lastly, (iv) benchmarking the predicted AEP loss against other studies and analysing differences. The paper is organised into the following structure: Section 2 presents details of the 2D computational model used, the mesh dependency study and the computational domain used in simulations. Section 3 presents the method of incorporating roughness into the model, and the results of simulating different levels of roughness on the LE of a NACA 63_3-618 aerofoil has on lift, drag and the laminar-turbulent transition characteristics of the aerofoil. The impacts of bypass transition are also addressed in Section 3. Section 4 describes the incorporation of the predicted aerodynamic characteristics for eroded aerofoils into a blade element momentum (BEM) model of the DTU 10-MW RWT, the generation of power curves and calculation of predicted AEP loss for the configuration in this study. The predicted AEP loss is benchmarked against predicted losses from other studies and an analysis of the approaches across the studies is made in Section 5, and conclusions are presented in Section 6.

The AEP analysis method as described in detail through Sections 2 to 4 in this paper is summarised in Figure 1. The section in this paper that each part relates to is included in brackets.

2 | 2D CFD SIMULATION DEVELOPMENT AND VALIDATION

This section is split into subsections which contain details of the setup for computational analyses, the results of a mesh dependency study and validation of the resulting computational domain.

2.1 | Computational setup

In normal operation, the majority of a wind turbine blade can be assumed to be in a two-dimensional (2D) flow, where radial effects are negligible. Therefore, a series of 2D CFD simulations were used to obtain lift and drag coefficient data for the aerofoil in a clean state, and with different levels of simulated roughness. Erosion effects are most prominent near to the tip, where relative velocity is the highest, and the kinetic energy of impacting particles is greatest. A smaller aerofoil chord and thickness in this region also amplifies these effects as relative changes to the aerofoil shape are greater than further inboard. Common aerofoil maximum thickness-to-chord ratio for near tip aerofoils of offshore wind turbines is in the order of 18%[4]; hence, a NACA 63_3-618 aerofoil was used. The NACA 63_3-618 aerofoil was used in place of the FFA-W3-241 aerofoil since coordinate and polar data is openly available for the NACA section and its properties are well defined in published literature, aiding method validation. As will be shown in Section 4.1, the performance of this blade section is very similar to, and therefore representative of the performance of the FFA aerofoil used on the DTU 10-MW RWT.

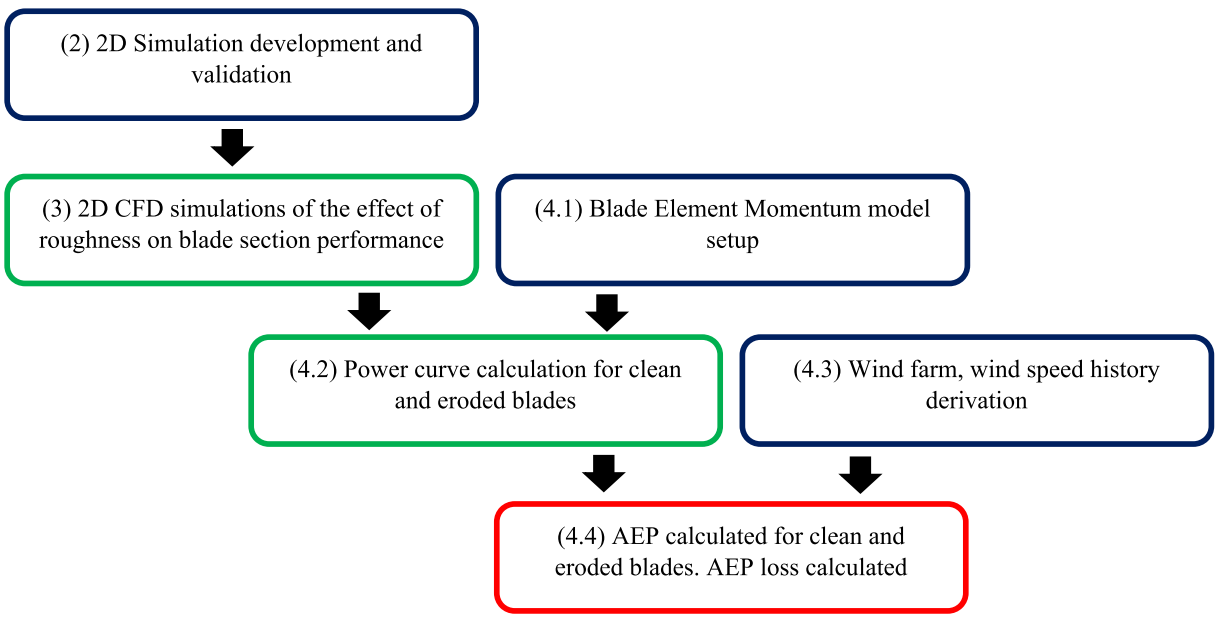

FIGURE 1 Flow chart of steps taken in conducting the AEP analysis

Pointwise, V18.3 was used to establish the mesh for the simulation domain using an O-grid. The resultant structured mesh was produced from grid lines that extended normal to the aerofoil surface from each of the nodes defining its shape to the outer radius of the calculation domain. The near-wall cell height was set to give y^+ values close to unity so that the viscous sub-layer is resolved.

When the DTU 10-MW RWT is operating at a rated wind speed of 11.4 ms^{-1}, the turbine rotates at 9.6 RPM. The blade radius is 89.15 m which gives a blade tip speed of 89.62 ms^{-1}. This gives a relative velocity freestream boundary condition for the calculation of U_∞ 90.35 ms^{-1}. Subsequently, for an aerofoil chord length, c, of 1 m and values of ρ and μ for air under at ISA sea level values, the Reynolds number used in the following mesh dependency study and simulations was 6.4×10^6.

CFD simulations were conducted using Ansys Fluent V19.2.[18] Accurate resolution of the boundary layer around the aerofoil section is critical for the calculations and so the four-equation Transition SST turbulence model was used throughout. This model allows boundary layer transition to be accurately captured by incorporating Equations for intermittency, γ, and momentum thickness Reynolds number, Re_θ, with the standard SST k-ω model.

Freestream boundary conditions were defined according to Equations 1 and 2.[19]

$$k_\infty = U_\infty^2 \times 10^{-6} \tag{1}$$

$$\omega_\infty = \frac{5U_\infty}{c} \tag{2}$$

The symbols above, k, U, ω and c represent the turbulent kinetic energy, velocity, specific dissipation rate and chord length, respectively. The subscript ∞ represents a freestream condition. The value '5' in Equation 2 is a constant specified in the model of Spalart et al.[19]

CFD models suffer from numerical diffusion effects,[19] and so in many cases inlet values of k and ω are significantly higher than those that would be experienced at the aerofoil, and less controllable as turbulence is damped out as flow advances through the computational domain. In order to provide additional control of the turbulent intensity, and to prevent damping of turbulence levels to zero, the work of Spalart et al. was adopted to constrain the freestream decay of k and ω. In the freestream, the turbulent intensity is set according to Equation 3.

$$TU_\infty = \frac{100}{U_\infty}\sqrt{\frac{2k_\infty}{3}} \tag{3}$$

The symbols in Equation 4 have the same meaning as in Equation 2 with the addition of TU representing the turbulent intensity. By substituting Equation 2 into Equation 4, this can be simplified to show that freestream turbulent intensity is independent of freestream velocity and has a value of 0.08165%.

Adding additional source terms into the transport equations for turbulent kinetic energy and specific dissipation rate cancels out the respective destruction terms in the freestream, meaning that the above turbulent intensity is maintained as constant throughout the freestream. As turbulent kinetic energy and specific dissipation rate around the aerofoil differ by orders of magnitude to freestream values, the impact on natural turbulence generation at the aerofoil surface is minimal.

2.2 | Mesh dependency study

Table 1 shows the baseline mesh parameters that were chosen to give a high-density mesh close to the aerofoil surface, following recommendations in the Ansys Fluent guide,[20] the growth rate in all mesh dependency studies was kept constant at 1.07. Based on calculations to achieve an approximate y^+ value of 1, a first cell height of 1×10^{-6} m was used. The reference chord length used in the mesh dependency study and

TABLE 1 Initial mesh parameters

Nodes around aerofoil	700
First cell height	1×10^{-6} m
Growth rate	1.07
Maximum cell height	0.5 m
Domain radius (chord lengths)	50
Number of cells	117 800

subsequent simulations was 1 m. An O-domain was used for this study, with the domain radius set as 50 chord lengths. The Reynolds number of the studies detailed herein was 6.4×10^6.

The parameters shown in Table 1 were used as the basis for a mesh dependency study. The aerofoil was set at a constant angle of attack of $\alpha = 7^\circ$ for all aspects of the study. The sensitivity of the predicted coefficients of lift and drag, as calculated by Ansys Fluent (defined according to Equations 4 and 5) to variations in the number of nodes normal to and along the aerofoil were investigated.

$$c_l = \frac{l}{\left(\frac{1}{2}\right)\rho U_\infty^2 c} \tag{4}$$

$$c_d = \frac{d}{\left(\frac{1}{2}\right)\rho U_\infty^2 c} \tag{5}$$

To assess sensitivity to the number of nodes normal to the aerofoil, the maximum cell height was varied from 1.5 to 0.25 m while the growth rate was kept constant at 1.07. The results are shown in Table 2.

Coefficients c_l and c_d were shown to converged to within 0.001 and 0.0001, respectively, for a maximum cell height of 0.5 m. Above this the accuracy of aerodynamic coefficient prediction decreased, and below this, there was no improvement in the predictions for a denser grid. A maximum cell height of 0.5 m was used throughout the rest of this paper.

The position of the transition point on the suction side of the aerofoil was observed in addition to c_l and c_d when assessing the sensitivity of the solution to the number of nodes used to define the aerofoil. The number of nodes was varied from 172 to 1404, where nodes were clustered towards the leading and trailing edges of the aerofoil and each had 277 nodes normal to the aerofoil surface. Results are shown in Table 3 and Figure 2.

The transition location was determined from the step change in skin friction coefficient, as defined in Equation 6, shown in Figure 2. Increased turbulence causes higher energy fluid elements to be transported towards the surface resulting in a higher near surface velocity and increased skin friction.[21] From Figure 2, it can be seen that when the number of aerofoil nodes is too low, transition is predicted closer to the LE. The peak value of the predicted skin friction coefficient is shown to be insensitive to the number of aerofoil nodes used. The magnified view shows that the predicted position of the transition point becomes insensitive to the number of aerofoil nodes when more than 1000 nodes are used. The lift coefficient prediction in Table 3 converged to within 0.001 with a change in c_d of only 0.0001 when more than 1000 aerofoil nodes are used; therefore, 1404 aerofoil nodes were selected for use in all further calculations.

$$c_f = \frac{\tau_W}{\frac{1}{2}\rho_\infty v_\infty^2} \tag{6}$$

where c_f is the skin friction coefficient, τ_W is the wall shear stress and ρ_∞ and v_∞ are the freestream density and velocity, respectively.

TABLE 2 Grid convergence results for varied maximum cell height for a NACA 63_3–618 aerofoil at $\alpha = 7^\circ$ and $\mathrm{Re} = 6.4 \times 10^6$

Maximum cell height (m)	Number of nodes normal to aerofoil	Number of cells	c_l	c_d
1.5	226	158 200	1.301	0.0118
0.75	249	174 300	1.302	0.0118
0.5	277	193 900	1.306	0.0116
0.25	366	256 200	1.306	0.0116

TABLE 3 Grid convergence results for altered number of aerofoil nodes for a NACA 63_3–618 aerofoil at $\alpha = 7^\circ$ and $\mathrm{Re} = 6.4 \times 10^6$

Number of aerofoil nodes	Number of cells	c_l	c_d
172	47 472	1.281	0.0146
348	96 048	1.291	0.0123
700	193 200	1.305	0.0116
1052	290 352	1.306	0.0115
1404	387 504	1.306	0.0114

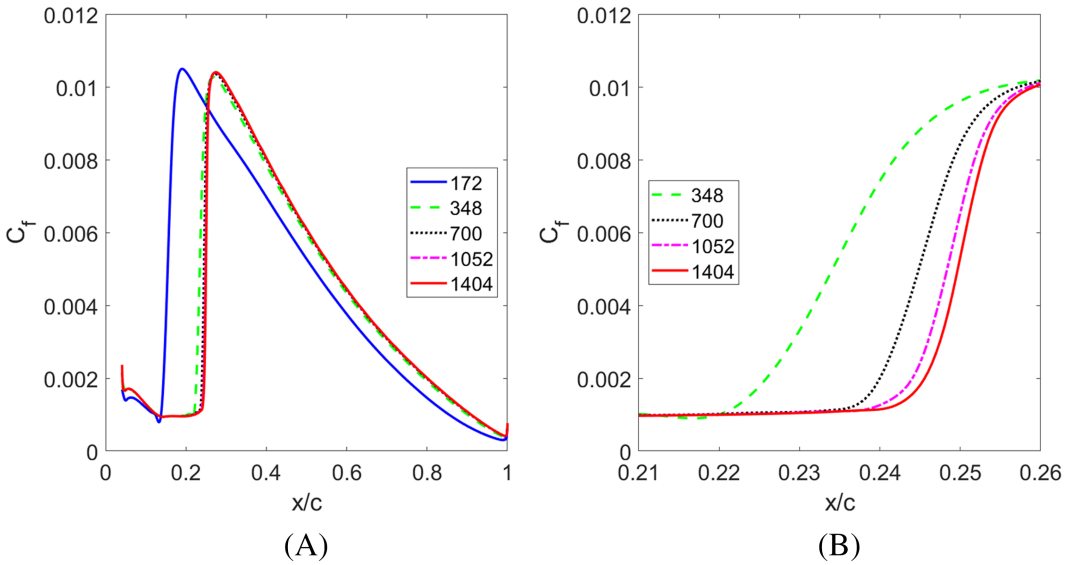

FIGURE 2 Variation of suction side skin friction coefficient with number of aerofoil nodes over (A) the full chord length and (B) magnified between 21% and 26% of the chord length

TABLE 4 Final mesh parameters

Nodes around aerofoil	1404
First cell height	1×10^{-6} m
Growth rate	1.07
Maximum cell height	0.5 m
Domain radius (chord lengths)	50
Number of cells	387 504

The final mesh parameters used in the simulations following the mesh sensitivity study are summarised in Table 4. Images of the mesh and the domain are shown in Figure 3.

2.3 | Simulation domain validation

In order to validate the CFD method using the mesh parameters in Table 4, an incidence sweep between aerofoil angles of attack of -15° and 15° was carried out at a Reynolds number of 6.4×10^6. The results for lift and drag coefficient were compared with aerodynamic characteristic data from Abbott and Von Doenhoff at $Re = 6 \times 10^6$ [22] and Xfoil simulations. The Xfoil simulations were run under a free transition model with an Ncrit value of 9, at a Reynolds number of 6.4×10^6. The comparisons are shown in Figure 4A,B.

Figure 4A shows excellent agreement for C_l with both the sets of reference data. Divergence of the CFD results from the experimental data at the higher angles of attack is attributed to an increase in three dimensional effects in the experiments at higher α, which are not captured in the 2D CFD simulations. Similarly, Figure 4B shows excellent agreement exists for C_d. The results shown in Figure 4 validate the CFD approach used in this study.

3 | 2D CFD SIMULATIONS OF THE EFFECT OF ROUGHNESS ON BLADE SECTION PERFORMANCE

Erosion is a disorderly and random process and is a challenge to accurately model using CFD. One of two approaches are commonly taken. The first, as used by Bak et al.[11] and Schramm et al.[8] is to attempt to model the material loss by modifying the aerofoil geometry in the LE region. However, it is difficult to model the fine details of distributed roughness using this method. The second approach involves using a conversion

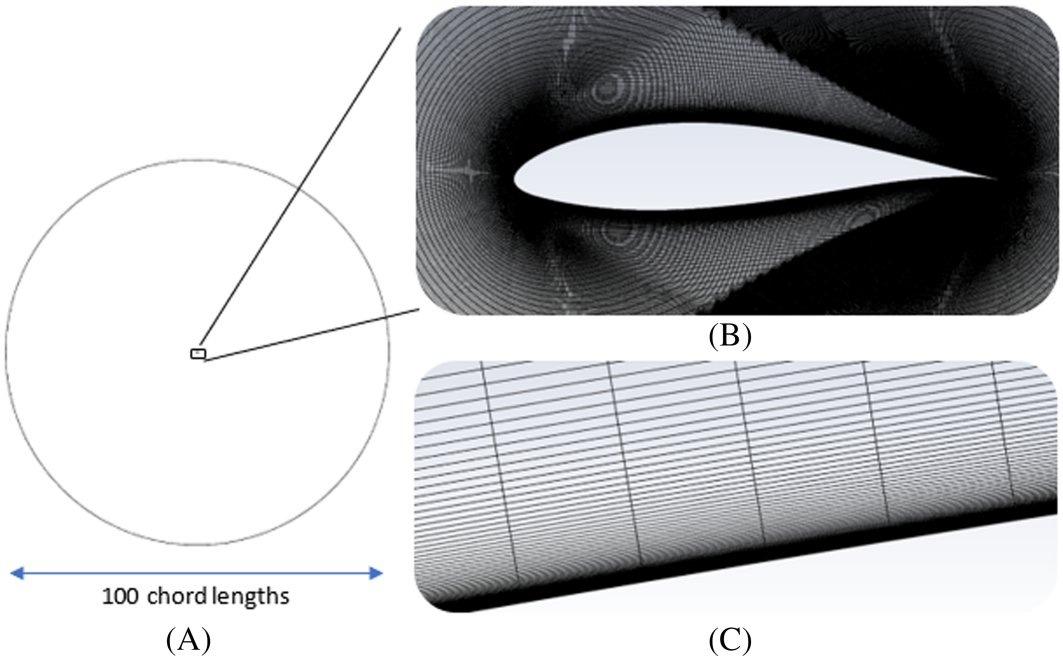

FIGURE 3 Resulting domain and mesh for simulations: (A) whole domain, (B) around aerofoil and (C) near aerofoil surface

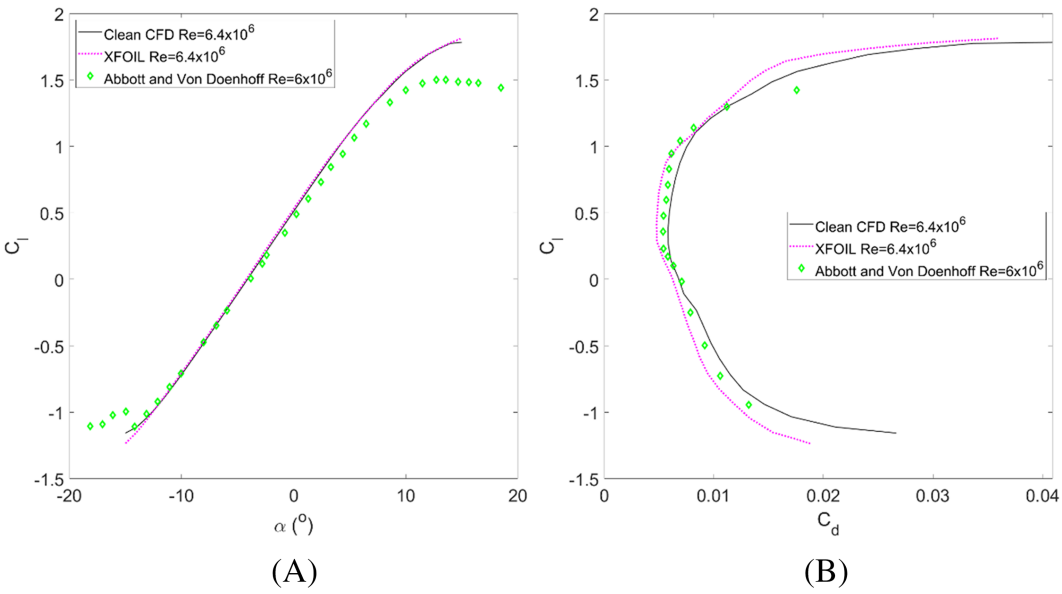

FIGURE 4 Comparisons of (A) c_l versus α and (B) c_l versus c_d for a NACA 63_3-618 aerofoil at comparative Reynolds numbers

factor, η, to scale the geometric roughness height to an equivalent sand grain roughness, with the conversion factor derived from the geometry and density of the roughness elements. While an equivalent sand grain roughness does not physically represent erosion, it can be used in conjunction with experimental testing, for example, Maniaci et al.,[23] to tune a computational model. The output then is a much more versatile model from which simple changes to the equivalent sand grain roughness can be used to test a wide variety of cases. A novel approach of combining the two methods was taken by Papi et al.,[12] with the benefit of being able to incorporate roughness within an eroded region. In this study, an equivalent sand grain roughness approach has been taken.

There is a lack of consensus in literature as to what conversion factor should be used to obtain an equivalent sand grain roughness, ε, based on the mean roughness height, R_a, owing to it being largely dependent on the geometric shape of the roughness elements. Different studies have used conversion factors spanning 4.5 to 6.5.[24–26] Owing to a lack of knowledge of the roughness distribution and the geometric profile of

roughness elements of the erosion distribution used in this study, it was not possible to develop a more accurate value based on Dirling's correlation,[27] therefore a value of $\eta = 5.5$ was used.

$$\varepsilon = \eta R_a \tag{7}$$

The work of Veraart[6] was used to determine the erosion affected area around the LE of the blade and the mean geometric height of the roughness elements. Veraart determined these parameters from a series of rain erosion tests and subsequent statistical analyses. From these tests, an impingement region along the first 4% of the aerofoil from the LE on both suction and pressure sides was seen, and so represents the roughness coverage used in the following simulations. Similarly, with the mean depth having been taken over the total coverage area, this mean depth was converted to an equivalent sand grain roughness and applied over the whole coverage area in simulations. The geometric roughness heights (erosion depths) used, and their equivalent sand grain roughness's are shown in Table 5.

In validating the clean case, a low level of equivalent sand grain roughness, 25 μm, was applied to all of the aerofoil surfaces to tune the lift and drag coefficients towards values of reference data. CFD simulations were run for angles of attack ranging from −15° to 15° in increments of 1° with the results shown in Figure 5A,B.

The effects that increased roughness had on the lift and drag coefficients can be seen in the above Figures 5A,B, with the expected decrease in lift, and increase in drag as the roughness level increases. There is very little difference in c_l and c_d trends for the medium and heavy roughness cases. This suggests the occurrence of a critical roughness height, above which there is little further decrease in performance as roughness is increased. The influence of variable roughness levels can be seen also in the differences in C_l, which is shown in greater detail in the insert in Figure 5A, and c_d with respect to the clean case. Light levels of roughness, which may be representative of early stages of erosion, or erosion further from the blade tip, appear to have little to no effect. Conversely, medium and heavy levels show a clear separation, that is, an increase in C_d and a decrease in C_l at all angles of attack.

The lift and drag coefficient distributions in Figure 5 show the effect of bypass transition. As noted earlier, bypass transition occurs in the presence of aerofoil LE roughness, or erosion, and causes the transition from laminar to turbulent flow to occur earlier than for natural transition mechanisms.[13] The four-equation transition SST turbulence model used in this analysis is capable of capturing this effect. As the angle of attack of an aerofoil increases, if the LE roughness is sufficient, bypass transition can result in a large movement in the location of the transition point on the aerofoil surface to the location of the roughness This can be seen in Figure 5 where there is a sudden change in the values of lift and drag coefficient at angles of attack of around 4° for the medium and heavy roughness cases. This effect has been observed previously in the experiments of Ehrmann et al.[15]

TABLE 5 Conversion of geometric roughness heights used in simulations, and the respective equivalent sand grain roughness

Roughness level	Light	Medium	Heavy
R_a (mm)	0.0822	0.389	0.716
ε (mm)	0.4521	2.140	3.938

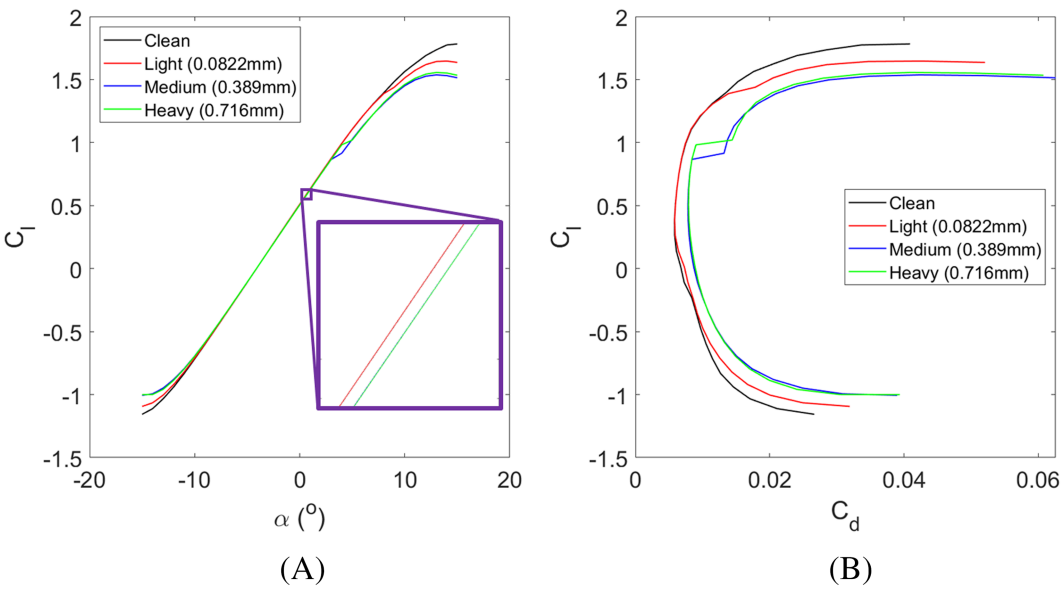

FIGURE 5 (*A*) c_l *versus* α and (*B*) c_l *versus* c_d for a NACA 63_3-618 aerofoil with varying levels of surface roughness over the first 4% of the chord at Re $= 6.4 \times 10^6$

The effect of LE roughness on the location of the transition point on the aerofoil's suction surface is further illustrated in Figure 6. In this Figure, the start location of the transition point in the CFD predictions was taken as the point where the turbulent viscosity increased above a value of 1×10^{-8} m^2 s^{-1}. As the flow along the aerofoil chord transitions from laminar to turbulent there is a rapid increase in turbulent viscosity from approximately zero. The 1×10^{-8} m^2 s^{-1} value was used to identify a location towards the start of transition.

The above results show that for the clean aerofoil, there is a gradual movement of the transition point on the suction surface from the trailing edge towards the LE, as the angle of attack increases. For a light roughness case, a sudden change in the location of the transition point occurs between $\alpha = 7^\circ$ and $\alpha = 8^\circ$ where the transition point moves from 22% to 4% of x/c. For the medium and heavy cases, a larger change in position from 45% to 4% of x/c occurs between $\alpha = 3^\circ$ and $\alpha = 4^\circ$.

The above predictions of transition locations on the aerofoil suction side and the bypass transition effects of simulated roughness are similarly shown in the plots of intermittency in Figure 7. These plots show the intermittency for all four roughness configurations at angles of attack of 0°, 5° and 10°, with the transition locations marked by stars. The same sudden forwards movement in transition location for cases with roughness above critical angles of attack can be seen for the light case at 10°, and the medium and heavy cases at both 5° and 10°.

The angles of attack around which roughness causes bypass transition lie within the standard operating region of the turbine, see Figure 12. The bypass-transition effect therefore has an important influence on the performance of the turbine as blade erosion occurs and needs be taken into account when analysing the impact of blade erosion on AEP.

4 | PREDICTING THE EFFECT OF LEADING EDGE EROSION ON THE AEP OF THE DTU 10-MW RWT

4.1 | Blade element momentum model setup

The CFD calculations described in the previous section were used to estimate the impact of the different erosion levels in Table 5, on the variations of c_l and c_d of a NACA 63_3-618 aerofoil section with angle of attack. The DTU 10-MW RWT has an FFA-W3-241 aerofoil section in the erosion affected section of the blade close to its tip. The lift, drag and transition properties of both aerofoils are compared in Figure 8.

By comparing lift and drag coefficient data of these two aerofoils, it can be seen that there are distinct similarities in the aerodynamic characteristics. Critically, this is more evident over the angles of attack the outer section of the blade would be operating at, see Figure 12, and those which are relevant to this study on AEP. This comparison shows that the NACA 63_3-618 is sufficiently representative of the FFA-W3-241 to provide realistic predictions of the DTU 10-MW RWT operation when simulation results are applied directly to the FFA aerofoil. Predicted percentage changes in c_l and c_d due to erosion at each angle of attack calculated for the NACA 63_3-618 section were applied to clean polar data for the FFA-W3-241 section. This approach was used to produce new polar data sets for the FFA-W3-241 section for the light, medium and heavy roughness cases shown in Table 5.

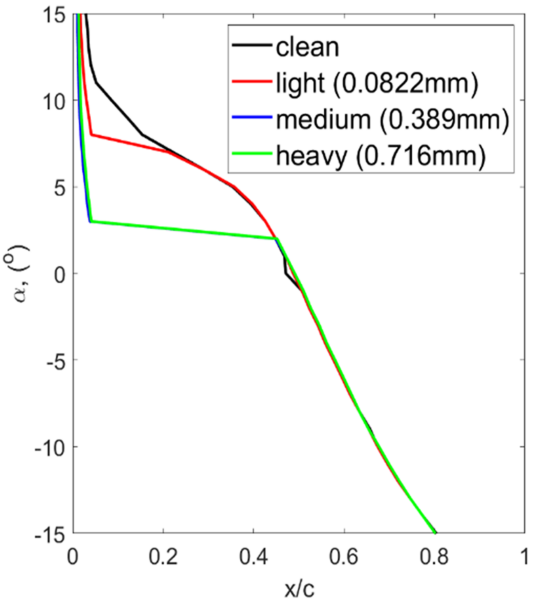

FIGURE 6 Suction side transition point variation across roughness levels for the NACA 63_3-618 at Re $= 6.4 \times 10^6$

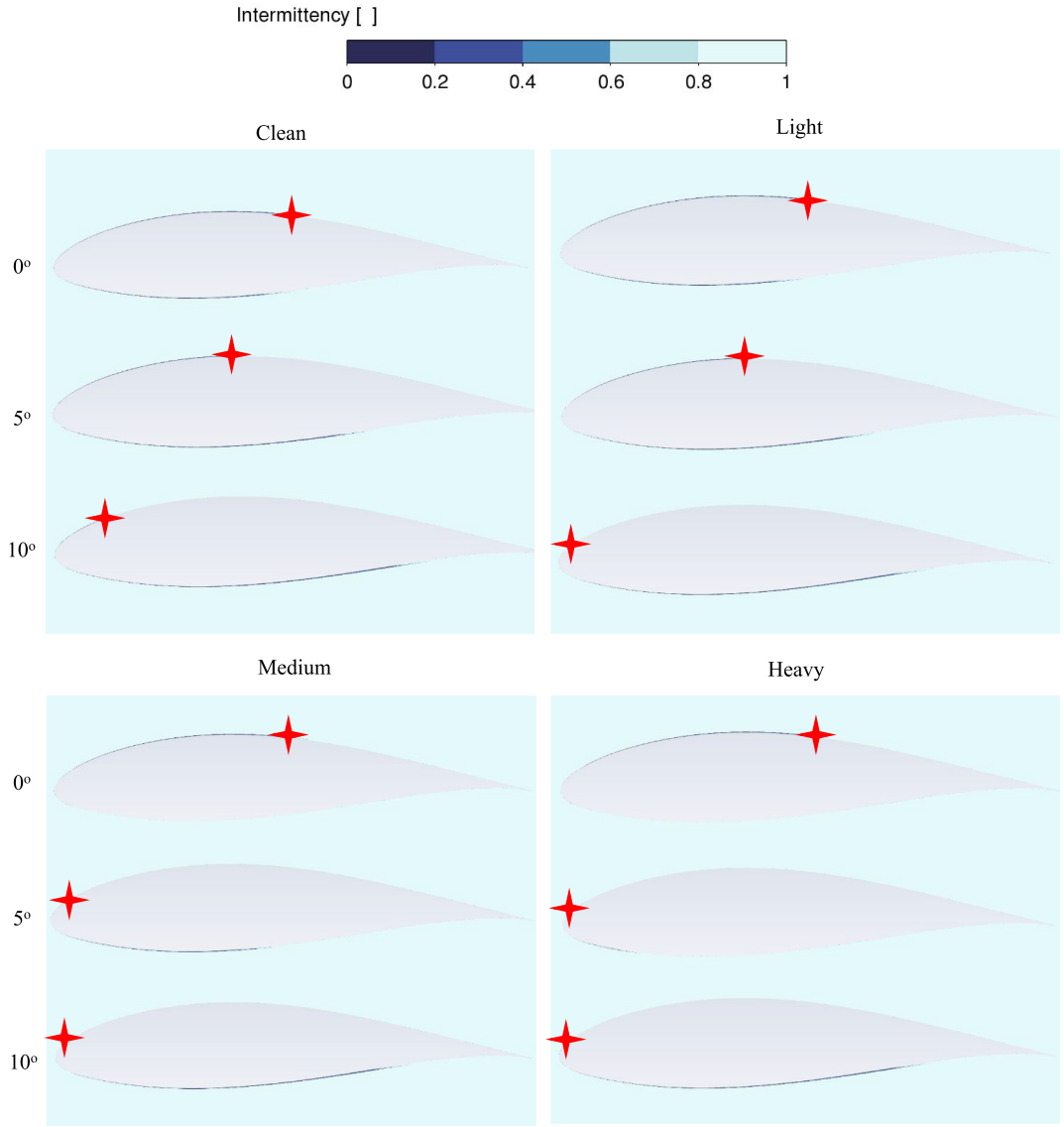

FIGURE 7 Contour plots of intermittency for clean-top left quadrant, light-top right, medium-bottom left, and heavy-bottom right roughness configurations. Each configuration shows $\alpha = 0^\circ$, 5°, and 10° from top to bottom respectively. Suction surface transition points are marked by a red star

BEM code Xturb[28] was adapted to contain geometric and polar data for the DTU 10-MW RWT in clean and eroded configurations. The inbuilt Viterna correction[29] of Xturb was used to extrapolate the derived lift and drag data to higher angles of attack. At $\alpha = 90^\circ$, a value of $c_{d,max} = 1.98$ was taken on the assumption that the 2D aerofoil acts as a rectangular flat plate of infinite aspect ratio.[30] For the eroded blade, in addition to the aerofoil sections that constitute the clean blade, as expressed in the definition of the DTU 10-MW RWT,[31] the polar data for the three eroded sections was included. The locations of the additional aerofoil sections in the eroded blade are shown in Table 6, where the locations of eroded sections were derived from the work of Veraart. While there is a difference in the rating of the turbine used in Veraart's study, 2.5 MW, and the work detailed here, 10 MW, it can be assumed that the spanwise penetration of erosion would be similar, owing to similar tip-speed ratios being utilised across different sized turbines.[32] Aerofoil blending over 5% of the aerofoil section length was enabled in the BEM model to give a gradual transition of polar data between sections. Tip and root loss factors were also incorporated.

4.2 | Power curves

The BEM code was run at wind speed intervals of 0.1 ms^{-1} from the cut-in velocity of 4 ms^{-1} to the cut-out velocity of 25 ms^{-1}, in order to generate power curves for the clean and eroded blade cases. The control strategy of the DTU 10-MW RWT was incorporated to properly represent

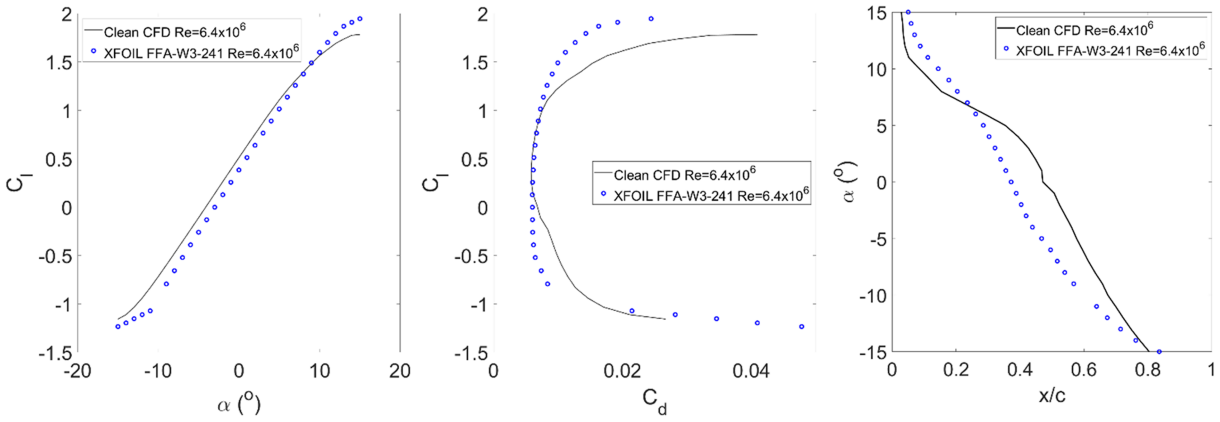

FIGURE 8 Comparison of aerodynamic coefficients (A) c_l versus α, (B) c_l versus c_d and (C) suction side transition point for NACA 63_3-618 and FFA-W3-241 aerofoils

TABLE 6 Radial location of additional aerofoils along the blade in the rough configuration

Aerofoil	Radial location (r/R)
FFA-W3-241-light	0.85–0.87
FFA-W3-241-medium	0.87–0.95
FFA-W3-241-heavy	0.95–1

the turbine. At the start of Region II, RPM is constant as wind speed increases until an optimal tip speed ratio (TSR) is achieved, while changes to the inflow angle are accommodated by changes to blade pitch. Once TSR is optimal, RPM is increased up to its rated level, with TSR maintained as constant, and blade pitch also kept constant. In Region III, power is held constant at the turbine's rated level by altering blade pitch and holding RPM at its rated level. The resulting power curves are shown in Figure 9.

These figures show the decrease in the power produced at a given wind speed caused by leading-edge erosion (LEE) within Region II. For a turbine with rough blades, the rated power is achieved at a higher rated velocity than for the clean case. The turbine requires a higher wind speed to increase lift on the blades and account for losses caused by erosion. Upon achieving the rated power, the blade pitch is altered to reduce torque so as not to exceed the rating of the turbine. Once rated power is achieved, it is maintained across higher wind speeds, independent of the blade condition, thus mitigating against erosion in Region III. Region I is before the cut-in speed of the turbine and so there is zero turbine power output in this region.

4.3 | Anholt wind farm annual wind distribution

The wind speed history used in this study was 10-min averaged LIDAR data from the Anholt offshore wind farm.[33] The available data spanned 2 years, thus capturing seasonal variations. The measurements were made at a height of 116 m above sea level, very close to the 119 m hub height of the DTU 10-MW RWT. Data was sorted into discrete 0.1 ms^{-1} velocity bins. This information was used to determine the proportion of a typical year that the wind farm was exposed to each wind speed. This data are represented in Figure 10 alongside the Weibull distribution that was generated from the data. The parameters for the Weibull distribution were determined from the raw data as a mean wind speed of $c = 10.73\ ms^{-1}$ and a shape factor of $k = 2.22$.

4.4 | Annual energy production

The annual wind distribution was integrated with the clean and eroded power curves from Figure 10 between the cut-in and cut-out velocities, as shown in Equation 8. This generates two values for AEP for the clean and eroded cases, allowing the reduction in AEP due to erosion to be evaluated from the difference between these predictions.

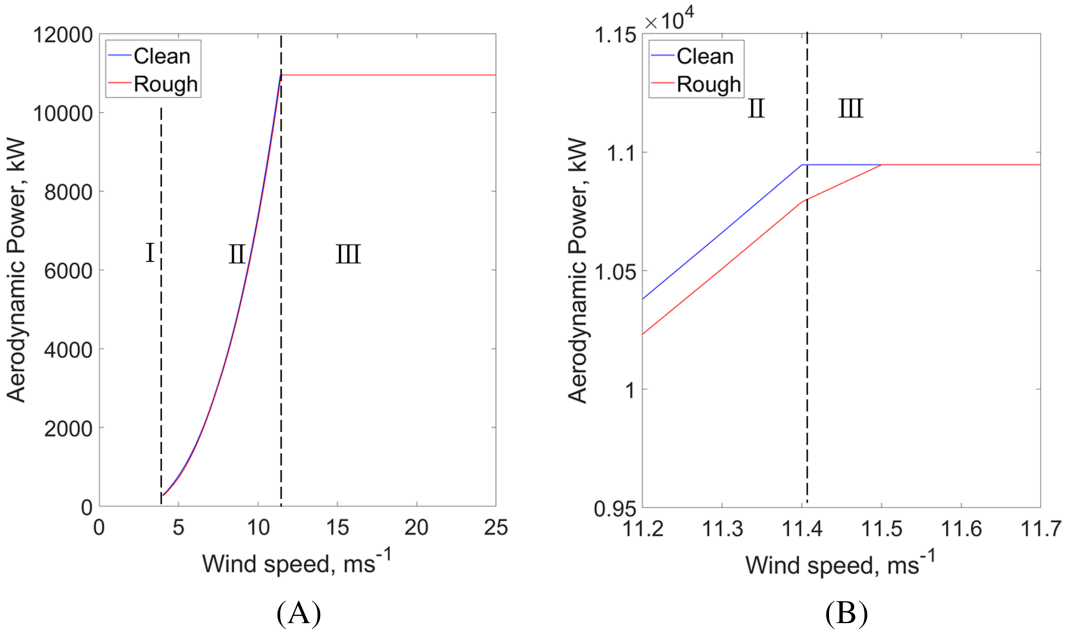

FIGURE 9 Power curves for the DTU 10-MW RWT in clean and rough configurations, with Regions I–III for the clean case labelled (A) over the turbine operating range and (B) magnified at the boundary of Regions II to III

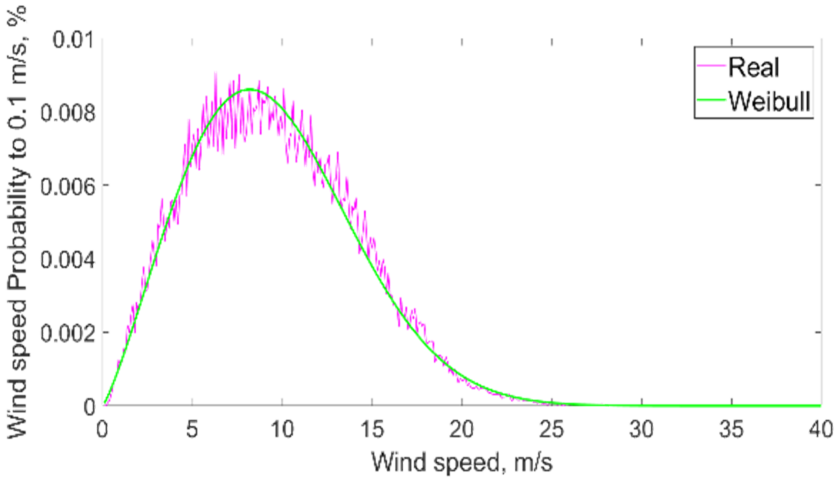

FIGURE 10 Real and Weibull wind distributions for Anholt offshore wind farm

$$AEP = \sum_{V_{cutin}}^{V_{cutout}} P_v t_v \tag{8}$$

The AEP for the DTU 10-MW RWT with the Anholt wind distribution was predicted to be 50.88 GWh for the turbine with clean blades and 50.53 GWh with rough blades. This corresponds to an AEP loss of 0.70%.

As noted earlier, the DTU 10-MW RWT controller means that the impact of blade erosion on turbine power output only influences Region II of the turbine's operation and a portion of Region III above the rated wind speed for a clean blade (Figure 9). This is due to the power loss in the eroded case causing a rated power not being achieved until a new, higher rated wind speed. This is further illustrated in Figure 11A,B which show the effect of erosion on turbine energy output.

With the Anholt wind data, the turbine spends the greatest portion of time operating in Region II. It operates in this region for 56.1% of the total operating time, which accounts for 42.25% of total energy produced. During this period, the eroded section of the blade is almost always operating at an angle of attack that lies beyond the onset angle for bypass transition, as expressed in Figure 12.

The above figure shows the percentage of time that the outer 15% of the blade span spends operating at a specific angle of attack within Region II for the DTU 10-MW RWT and a wind distribution from Anholt wind farm, consisting of data points every 0.25°. The *y*-axis shows the percentage of time of total operation over a year. Vertical lines, representing the angles for the onset of bypass transition were added in order to show that the outer 15% of the blade, where roughness was simulated, operates above the angles to trigger bypass transition calculated for almost the whole of Region II. It can then be seen that in this analysis, the detrimental effect of bypass transition has an important impact on the turbine's performance for upwards of 50% of its operating time, further underlining the importance of accounting for the presence of bypass-transition in the AEP analysis.

5 | BENCHMARKING AND COMPARISON OF PREDICTED AEP LOSS

There are a range of environmental and operational factors which influence studies on wind turbine AEP. These mean that without a quantitative understanding of the relationships between erosion characteristics and their impacts on AEP, direct comparisons with other studies may be harder to interpret. Similarly, it has been shown by Campobasso et al.[34] that there are significantly different aerodynamic interactions when modelling roughness as individual elements or distributed over the surface, introducing further uncertainties. A purpose therefore of Table 7 is to highlight some of the characteristics modelled in recent studies to suggest where variations may result in the different predicted AEP losses. It should be

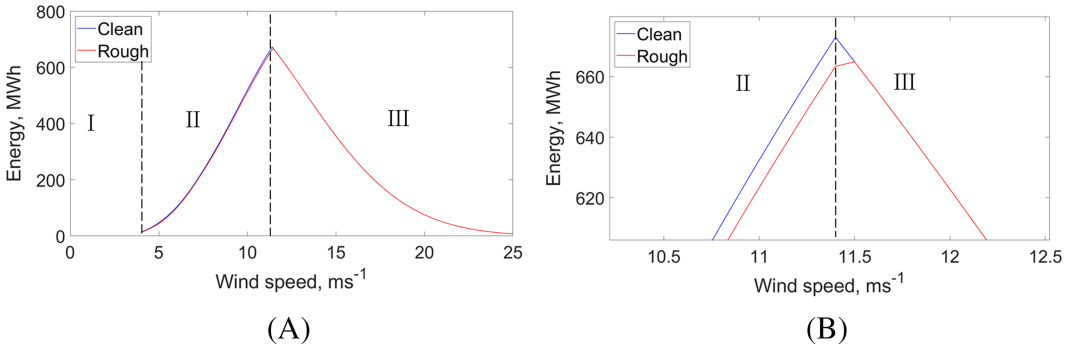

FIGURE 11 Energy curves for the DTU 10-MW RWT in clean and rough configurations, with Regions I–III for the clean case labelled (A) over the turbine operating range and (B) magnified at the transition from Regions II to III

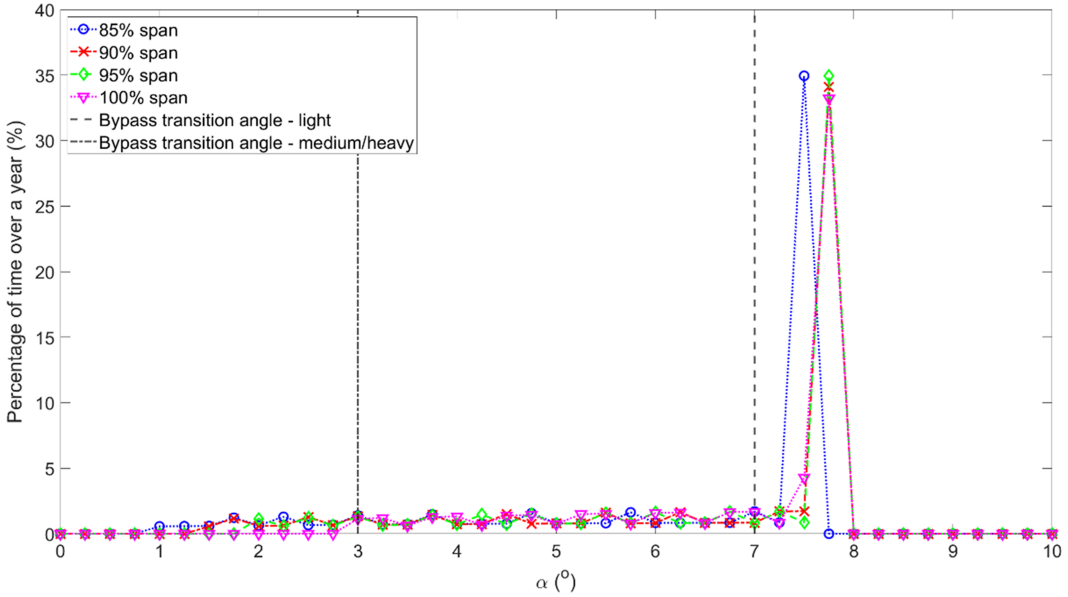

FIGURE 12 Angles of attack at intervals of 0.25° experienced over a year of operation for the DTU 10-MW RWT using a wind distribution from Anholt offshore windfarm in Region II of operation for the outer 15% blade span. Trend lines are included for ease of interpretation

TABLE 7 Comparison of AEP loss values reported in recent studies

Author	Year	Predicted AEP loss	Erosion characteristics modelled
Present work	2021	0.70%	Equivalent sand grain roughness in CFD for geometric roughness heights ranging from 0.08–0.7 mm, increasing towards tip, applied to 4% of the chord from the LE to the outer 15% of the blade
Papi et el.[12]	2020	0.87%	Probability density functions utilising data ranges of erosion depth, roughness height, and chord and span coverages from published studies to derive a mean AEP loss
Bak et al.[11]	2020	0.5%–3%	Stepped profiles in CFD for erosion of depths of 0.1%–0.2% of chord length, applied up to 1% of the chord from the LE to the outer 10%–30% of the blade
Eisenberg et al.[7]	2018	1.7%	Sareen et al.[4] 4C erosion level applied to the outer 10% of the blade, with chord coverage unspecified
Han et al.[10]	2018	2%–3.7%	Equivalent sand grain roughness in CFD for geometric roughness heights ranging from 0.1–0.3 mm applied between 10–50% of the chord from the LE to the outer 29.3% of the blade
Veraart[6]	2017	0.5%–1.8%	Experimental analysis for erosion depths ranging from 0.08–0.7 mm, increasing towards tip, applied to 4% of the chord from the LE to the outer 15% of the blade
Schramm et al.[8]	2017	7%–8%	Sareen et al.[4] erosion level 5C applied to an unspecified chord length from the LE (Figure 6 suggests 1%) and an unspecified span coverage (modified aerofoils suggests the outer 29.3%). Pitch regulation wasn't applied after rated power
Langel et al.[9]	2015	1.7%–4.5%	Equivalent sand grain roughness in CFD for a geometric roughness height of 0.29 mm, applied to 5% of the chord from the LE. Span coverage not specified
Sareen et al.[4]	2013	4%–24%	Experimental analysis for erosion depths ranging from 0.5–3.8 mm, applied between 1%–3% of the chord from the LE along entire span

noted that other influencing factors, such mean wind speed, which accounts for the variability in the results of Veraart and Langel et al., are not referenced here.

The earlier studies included in Table 7 show predicted reductions in AEP due to blade erosion of several percent. However, in recent years, as service experience has grown, more information is becoming available on the levels of erosion damage that are being experienced by current generation turbines operating in the offshore environment. The more recent studies by Veraart,[6] Bak et al.[11] and Papi et el.[12] have all taken advantage of this information. They have used it to inform the lower and more distributed levels of blade erosion damage more representative of the service feedback modelled in their calculations, compared to the earlier studies. The present study benefits from direct access to Ørsted and Siemens Gamesa Renewable Energy (SGRE) data on the blade erosion levels experienced on their turbines operating in the field. This and the other studies all show AEP reductions of typically less than 1% for offshore turbines after several years of operation. The 0.70% AEP reduction due to blade erosion calculated in this study is considered to be largely representative of what may be expected after the first few years of operation for a current generation offshore wind turbine under the conditions detailed in this paper. There are however a number of factors which induce uncertainty into this and other studies on LEE. Due to randomness in climatic conditions, such as wind and rain, and mechanical characteristics, such as defects, actual levels of erosion are quite variable. Confidence in the method prescribed here is due to the similarity in the predicted AEP loss between this computational study and the experimental study of Veraart, upon which the inputs were based, providing a reliable base from which further computations can be conducted.

6 | CONCLUSIONS

A wind turbine AEP calculation methodology has been described in this paper. The method is based on using Ansys Fluent CFD calculations validated for clean aerofoil sections, to calculate the effect on blade section performance when erosion damage is simulated on the LE. The work highlights the need to use a CFD method that is capable of capturing bypass-transition when it occurs on the suction surface of eroded aerofoil sections and quantifying the impacts of such. In the calculations, an equivalent sand grain roughness method was used to implement roughness around the LE of the aerofoil. The scale and distribution of the roughness used followed advice from Ørsted and Siemens SGRE based on their knowledge of typical blade erosion on current generation offshore wind turbines. The method was used to calculate the effect of blade erosion on AEP for the DTU 10-MW RWT using the NACA 63_3-618 blade section in the near-tip region. Polar distributions of lift and drag coefficients for a wide range of angles of attack were predicted by CFD. These data were then used together with a BEM model of the turbine using XTurb to produce turbine power curves with clean and eroded blades. The power curves were integrated with annual wind resource data from the Anholt offshore wind farm, to calculate AEP values for the turbine. The results showed that the blade erosion levels used in the study resulted in a 0.70% decrease in AEP, compared with the turbine when operating with blades in their uneroded state.

This result was compared with those from other studies. Several recently published studies have used erosion levels similar to those in this study. These have all predicted an effect of blade erosion on AEP reduction of less than 1%. Some earlier studies used much higher levels of erosion damage, which appear to be more severe than what is being observed on current generation turbines. AEP losses of several per cent were calculated in these studies. The value of 0.70% AEP loss due to erosion damage in this study is considered to be more representative of current generation offshore wind turbines after their first few years of operation for the environment considered in this study.

Bypass transition caused by roughness was assessed and shown to affect the aerodynamic efficiency of the turbine over a significant portion of operation. In over 56% of operating time, the blade is subject to the effects of bypass transition. This corresponds to over 42% of the total energy produced by the turbine.

ACKNOWLEDGEMENTS

The Authors would like to acknowledge the EPSRC Prosperity Partnership: A New Partnership in Offshore Wind, EP/R004900/1 for funding of this project. The authors would also like to acknowledge the support of Ørsted and Siemens Gamesa Renewable Energy.

PEER REVIEW

The peer review history for this article is available at https://publons.com/publon/10.1002/we.2697.

DATA AVAILABILITY STATEMENT

The data that support the findings of this study are openly available in Durham Research Online DATAsets Archive (DRO-DATA) at https://collections.durham.ac.uk/files/r27d278t071#.YVb4o7hKg2w Identifier: ark:/32150/r27d278t071.

ORCID

Aidan Duffy https://orcid.org/0000-0002-7780-6841
Grant Ingram https://orcid.org/0000-0001-7713-8735
Simon Hogg https://orcid.org/0000-0002-7118-9002

REFERENCES

1. Stehly T, Phillip B. *2018 Cost of Wind Energy Review*. Golden, CO: National Rnewable Energy Laboratory; 2020.
2. Moriarty P, Migliore P. *Semi-Empirical Aeroacustic Noise Prediction Code for Wind Turbines*. Golden, CO: National Rnewable Energy Laboratory; 2003.
3. Keegan MH, Nash DH, Stack MM. On erosion issues associated with the leading edge of wind turbine blades. *J Phys D Appl Phys*. 2013;46(38):383001.
4. Sareen A, Sapre CA, Selig MS. Effects of leading edge erosion on wind turbine blade performance. *Wind Energy*. 2013;17:1531-1542.
5. Gaudern N. A practical study of the aerodynamic impact of wind turbine lade leading edge erosion. *J Phys Conf Ser*. 2014;524(1):012031.
6. Veraart M. Deterioration in Aerodynamic Performance due to Leading Edge Rain Erosion, MSc Thesis, 2017.
7. Eisenberg D, Laustsen S, Stege J. Wind turbine blade coating leading edge rain erosion model: development and validation. *Wind Energy*. 2018;21(10):942-951.
8. Schramm M, Rahimi H, Stoevesandt B, Tangager K. The Influence of Eroded Blades on Wind Turbine Performance Using Numerical Simulations. *Energies*. 2017;10:(9):1420. https://doi.org/10.3390/en10091420
9. Langel CL, Raymond C, Hurley OF, Van Dam CP, Ehrmann RS, White EB, Maniaci D. Analysis of the imact of leading edge surface degradation on wind turbine performance, in *33rd Wind Energy Symposium*, Kissimmee, Florida, USA, 2015.
10. Han W, Kim J, Bumsuk K. Effects of contamination and erosion at the leading edge of blade tip airfoils on the annual energy production of wind turbines. *Renew Energy*. 2018;115:817-823.
11. Bak C, Forsting AM, Sorensen NN. The influence of leading edge roughness, rotor control and wind climate on the loss in energy production, in *The Science of Making Torque from Wind (Torque 2020)*, 2020, 1618, 052050.
12. Papi F, Balduzzi F, Ferrara G, Bianchini A. Uncertainty quantification on the effects of rain-induced erosion on annual energy production and performance of amMulti-MW wind turbine. *Renew Energy*. 2020;165:701-715.
13. Nagarajan S, Lele SK, Ferziger JH. Leading edge effects in bypass transition. *J Fluid Mech*. 2007;572:471-504.
14. Tani I. Boundary-layer transition. *Annu Rev Fluid Mech*. 1969;1(1):169-196.
15. Ehrmann RS, White EB. Effect of blade roughness on transition and wind turbine performance. *Wind Energy*. 2010;1-25.
16. Morkovin MV. Bypass transition to turbulence and research desiderata, *NASA*, *Lewis Research Centre Transition in Turbines*, 1985;161-204.
17. Major D, Palacios J, Maughmer M, Schmitz S. Aerodynamics of leading-edge protection tapes for wind turbine blades. *Wind Eng*. 2020;1452:1-21.
18. ANSYS, Inc. Ansys®Fluent, Release 19.2.
19. Spalart PR, Rumsey CL. Effective inflow conditions for turbulence models in aerodynamic calculations. *AIAA J*. 2007;45(10):2544-2553.
20. ANSYS. ANSYS Fluent theory guide, release 15.0, 2013.
21. Anderson J. *Fundamentals of Aerodynamics*. 2nd ed. McGraw Hill; 1991.
22. Abbott IH, Von Doenhoff AE. *Theory of Wing Sections: Including a Summary of Airfoil Data*. New York: Dover Publications, Inc.; 1959.
23. Maniaci DC, White EB, Wilcox B, Langel CM, van Dam CP, Paquette JA. Experimental measurement and CFD model development of thick wind turbine airfoils with leading edge erosion. *J Phys*. 2016;753(2):022013.
24. Adams T, Grant C, Watson H. A simple algoritm to relate measured surface roughness to equivalent sand grain roughness. *Int J Mech Mechatron*. 2012;1(1):66-71.

25. Cebeci T. *An Engineering Appproach to the Calculation of Aerodynamic Flows*. Springer; 1999.
26. Aupoix B, Spalart PR. Extensions of the Spalart–Allmaras turbulence model to account for wall roughness. *Int J Heat Fluid Flow*. 2003;24(4):454-462.
27. Dirling Jr RB. A method for computing roughwall heat transfer rates on reentry nosetips, in *AIAA 8th Thermophysics Conference*, Palm Springs, California, 1973.
28. Schmitz S. XTurb-PSU: a wind turbine design and analysis tool, The Pennsylvania State University, 2012.
29. Mahmuddin F, Klara S, Sitepu H, Hariyanto S. Airfoil lift and drag extrapolation with viterna and montgomerie methods. *Energy Procedia*. 2017;105:811-816.
30. Carvill J. 4.6.4 Drag coefficients for various bodies. In: *Mechanical Engineer's Data Handbook*. Elsevier Ltd; 1994.
31. Bak C, Zahle F, Bitsche R, Kim T, Yde A, Henriksen LC, Natarajan A, Hansen M. Description of the DTU 10-MW reference wind turbine, 2013.
32. Yurdusev MA, Ata R, Cetin N. Assessment of optimum tip speed ratio in wind turbines using artificial neural networks. *Energy*. 2006;31(12):2153-2161.
33. Ørsted. Offshore wind data. 2019. [Online]. Available: https://orsted.com/en/our-business/offshore-wind/wind-data
34. Campobasso MS, Castorrini A, Cappugi L, Bonfiglioli A. Experimentally Validated three-dimensional computational aerdynamics of wind turbine blade sections featuring leading edge erosion cavities. *Wind Energy*. 2021;1-22.

How to cite this article: Duffy A, Ingram G, Hogg S. The significance of bypass transition on the annual energy production of an offshore wind turbine. *Wind Energy*. 2022;25(4):772-787. doi:10.1002/we.2697